

Gradient vector flow with mean shift for skin lesion segmentation

Huiyu Zhou^{a,*}, Gerald Schaefer^b, M. Emre Celebi^c, Faquan Lin^d, Tangwei Liu^d

^a Queen's University Belfast, Belfast, BT3 9DT, United Kingdom

^b Loughborough University, Loughborough, LE11 3TU, United Kingdom

^c Louisiana State University, Shreveport, LA 71115, United States

^d Guangxi Medical University, Nanning 530021, China

ARTICLE INFO

Article history:

Received 24 October 2009

Received in revised form 1 August 2010

Accepted 7 August 2010

Keywords:

Image segmentation
Gradient vector flow
Mean shift
Convergence
Accuracy

ABSTRACT

Image segmentation is an important task in the analysis of dermoscopy images since the extraction of skin lesion borders provides important cues for accurate diagnosis. In recent years, gradient vector flow based algorithms have demonstrated their merits in image segmentation. However, due to the compromise of internal and external energy forces within the partial differential equation these methods commonly lead to under- or over-segmentation problems. In this paper, we introduce a new mean shift based gradient vector flow (GVF) algorithm that drives the internal/external energies towards the correct direction. The proposed segmentation method incorporates a mean shift operation within the standard GVF cost function. Theoretical analysis proves that the proposed algorithm converges rapidly, while experimental results on a large set of diverse dermoscopy images demonstrate that the presented method accurately determines skin lesion borders in dermoscopy images.

© 2010 Elsevier Ltd. All rights reserved.

1. Introduction

Malignant melanoma, the most deadly form of skin cancer, is one of the most rapidly increasing cancers in the world, with an estimated incidence of 68,720 and an estimated total of 8650 deaths in the United States in 2009 alone [1]. Early diagnosis is particularly important since melanoma can be cured with a simple excision if detected early.

Dermoscopy, one of the major tools for the diagnosis of melanoma, is a non-invasive skin imaging technique that involves optical magnification which makes sub-surface structures more readily visible compared to conventional clinical images [2]. This in turn reduces screening errors and provides greater differentiation between difficult lesions such as pigmented Spitz nevi and small, clinically equivocal lesions [3]. However, it has also been demonstrated that dermoscopy might lower the diagnostic accuracy in the hands of inexperienced dermatologists [4]. Therefore, in order to minimise diagnostic errors resulting from the difficulty and subjectivity of visual interpretation, the development of computerised image analysis techniques is of paramount importance [5].

Automatic border detection of lesions is often the first step in the automated or semi-automated analysis of dermoscopy images and is crucial for accurate diagnosis [6]. Image segmentation can be defined as the grouping of similar pixels (i.e. lesion and non-lesion pixels) in a parametric space. Segmentation algorithms include bal-

loons [7], distance potential force [8], diffusion snakes [9], gradient vector flow (GVF) [10] and its generalisation [11] and further developments [12,13]. GVF and its variants have been shown to work well by attracting the active contour towards object boundaries from a relatively large distance, while being capable of converging to object cavities. In recent years, numerous efforts have been made to provide potential solutions towards capture range or/and topological change problems. For example, a graph theory based approach was introduced by Li et al. [14] within the external force term in the snake model to perform automatic snake initialisation or splitting. Chuang and Lie [15] presented a downstream algorithm based on an extended GVF field model, where the downstream process starts with a set of seeds scored and selected by considering local gradient direction information around each pixel. Yang et al. [16] proposed a robust colour GVF snake model which combined robust estimation and colour gradients using a L_2E robust estimation. Vasilevskiy and Siddiqi [17] demonstrated a gradient flow model which can be used to maximise the rate of increase of flux of a vector field in a two- or three-dimensional domain. The main contribution of this work is the direction of the vector field along with its magnitudes. Paragios et al. [13] proposed an edge driven bi-direction geometric flow for boundary detection by combining the geodesic active contour flow [18] and the gradient vector flow model [10].

In this paper, we propose a new type of dynamic energy force for snakes by combining local GVFs with a mean shift strategy. The energy force starts with the calculation of force vectors in the image domain. The deformation of the region surrounded by the evolving boundary is constrained by the mean shift of the pixels

* Corresponding author. Tel.: +44 28 90971869; fax: +44 28 90971702.

E-mail addresses: andy4.11@yahoo.co.uk, H.Zhou@ecit.qub.ac.uk (H. Zhou).

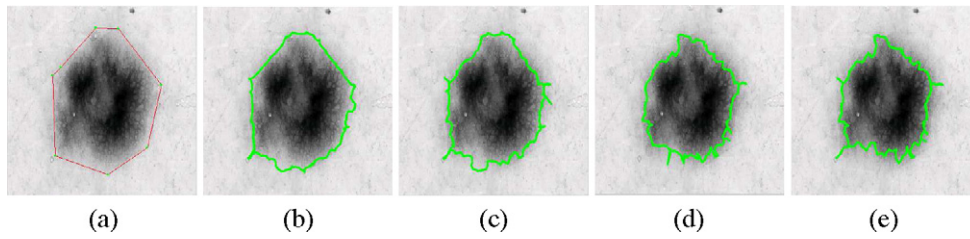


Fig. 1. Example of GVF segmentation: (a) initialisation (red), (b) image 10, (c) image 20, (d) image 30 and (e) image 40. The parameters used in this evaluation are $\alpha = 0.05$, $\beta = 0.01$, $\gamma = 1$, flow weight $\kappa = 0.6$. (For interpretation of the references to color in this figure legend, the reader is referred to the web version of the article.)

in the region. In other words, the evolution of the contour is not only driven by the gradient vector flows but also by the cumulative energy of the image region. This extended mean shift based GVF algorithm is versatile and flexible in that both local and global energy minimisation are achieved, leading to correct convergence against a severely noisy background.

The rest of the paper is organised as follows: In Section 2, the original GVF algorithm and its variants are introduced and discussed. Our proposed mean shift based GVF approach is described in Section 3. Section 4 presents extensive comparative results of the proposed scheme and conventional approaches. Finally, conclusions and future directions are given in Section 5.

2. GVF image segmentation

Snake (active contour) algorithms are used to detect object boundaries or edges given an initial guess of the evolving contours. The classical snake model considers a combination of internal and external energy, in which the boundary will stop evolving on the compromise of the two energy interactions. The internal energy term maintains smoothness and compactness of the curve shape, while the external energy term tunes the curve in order to be consistent with the inherent image gradients. Normally, the negative of the image gradient magnitude is used as the external energy; this indicates that larger gradient magnitudes will drive the evolution of the contour towards the real object boundaries [19].

The external energy force in the snake model is restricted to a small area surrounding the real boundary. If it is far from the real boundary, the snake will have difficulty in converging to the correct boundary. Xu and Prince [10] proposed a GVF map to represent the external energy force in the snake model. This GVF term is sensitive to the object boundaries or edges and hence effectively pulls the snake towards the real edges. Let a snake be a curve $\mathbf{x}(s) = [x(s), y(s)]$, $s \in [0, 1]$, which evolves in an image domain to reach a minimisation of the following energy function:

$$E(\mathbf{x}) = \int_0^1 \left[\frac{1}{2} \left(\alpha \left| \frac{\partial \mathbf{x}}{\partial s} \right|^2 + \beta \left| \frac{\partial^2 \mathbf{x}}{\partial s^2} \right|^2 \right) + E_{\text{ext}}(\mathbf{x}) \right] ds, \quad (1)$$

where α and β are the weights that dominate the tension and rigidity of the snake, respectively. The first order derivative $\partial \mathbf{x} / \partial s$ encourages stretching while the second order derivative $\partial^2 \mathbf{x} / \partial s^2$ leads to bending. The first two terms on the right-hand side of Eq. (1) are referred to as the internal energy of the snake, while the third term is the external energy that attains small values at feature points. In the presence of high gradients at image boundaries (e.g. step edges) the external energy is represented by $-\nabla(G_\sigma(x, y) * I(x, y))^2$ (where $*$ indicates the convolution operation). In the case of line drawings, $\pm G_\sigma(x, y) * I(x, y)$ is used instead, where G_σ is a two-dimensional Gaussian function with standard deviation σ .

To minimise $E(\mathbf{x})$, the contour has to be evolved by satisfying the following time-dependent function:

$$\gamma \frac{\partial \mathbf{x}}{\partial t} = \frac{\partial}{\partial s} \left(\alpha \frac{\partial \mathbf{x}}{\partial s} \right) - \frac{\partial^2}{\partial s^2} \left(\beta \frac{\partial^2 \mathbf{x}}{\partial s^2} \right) - \nabla E_{\text{ext}}(\mathbf{x}) = 0, \quad (2)$$

where γ is the coefficient component.

Classical snakes have two main problems: initialisation, and difficulty in handling topological changes. As a result, GVF is introduced for solving these problems. The external energy of Eq. (2) is replaced with a GVF field, $-\nabla E_{\text{ext}}(\mathbf{x})$, which is defined as the solution of the following partial differential equations:

$$\begin{cases} \mathbf{v}_t = \mu \nabla^2 \mathbf{v} - (\mathbf{v} - \nabla f) |\nabla f|^2, \\ \mathbf{v}_0 = \nabla f, \end{cases} \quad (3)$$

where \mathbf{v}_t is the partial derivative of \mathbf{v} against t , $\nabla^2 = \partial^2 / \partial x^2 + \partial^2 / \partial y^2$, and f indicates an edge map of the image that attains a large value at the feature points.

The values of μ and $|\nabla f|$ dominate the final settlement of the snake. For example, in the presence of intensive noise the regulator μ is usually set to be a large value so that the gradients of the boundary candidates can be enhanced. On the other hand, if $|\nabla f|$ is large, where the energy produced by the image edges becomes dominant, it will lead to forcing \mathbf{v} to be similar to ∇f . Fig. 1 illustrates an example of GVF segmentation, where the snake is near the real boundary but the segmentation accuracy needs to be improved.

3. Proposed mean shift based GVF algorithm

3.1. Problem formulation

When the GVF snake is finally settled, where the internal and external forces are balanced, one can have the Euler equation, expressed as

$$\alpha C''(s) - \beta C'''(s) + \gamma V = 0, \quad (4)$$

where α and β are the weighting parameters that are used to control the strength of the snake's tension and rigidity respectively, γ is a proportional coefficient and V is the external force. Practically, these three parameters are set to be constants within the equation. $C(s)$ is the contour that delineates the desired boundaries, and $s \in [0, 1]$.

Before exploring any improvement based on the original GVF platform, we rewrite Eq. (4) as

$$g_1(d)C''(s) - g_2(d^{-1})C'''(s) + g_3(d)V = 0, \quad (5)$$

where $g_1(d)$, $g_2(d^{-1})$ and $g_3(d)$ are the *weighting functionals* of the internal and external energy terms, respectively, and d is the Euclidean distance between the presumed centroid of the real boundary and the estimated one of the snake. In fact, if the snake is ideally placed on the real boundary, then they both most likely share a common centroid in addition to the merging of the contours. As a result, it is common practice to regard the Euclidean distance between the centroids as an index of *proximity*. However, we do not

take into account the case where each weighting functional has two or more combinatorial variables, i.e. $g_1(d, \alpha)$. This particular case is a more complicated mechanism which is beyond the scope of this paper. Note that there exists a significant difference between the functional $g_1(d)$ and $g_2(d^{-1})$ in terms of the variables. This is due to the opposite behaviour of d in the elasticity and rigidity terms, where the former is dominant in the energy function when d is large or the latter plays a key role when d is small [20,21].

Alternatively, we can use the simplified version of Eq. (5) as

$$\tilde{g}_1(d)C''(s) - \tilde{g}_2(d^{-1})C'''(s) + \gamma V = 0, \quad (6)$$

which is dependent on the assumption that, as the snake evolves, the GVF field remains stationary (this assumption may reduce the computational requirements of the optimisation). Evidence shows that this assumption holds strictly in static images but might fail in dynamically variable images, e.g. motion artefacts, occluded images, etc.

Suppose that $\tilde{g}_1(d)$ and $\tilde{g}_2(d^{-1})$ have continuous derivatives. Then, one has a Taylor series, which can be defined as

$$\begin{cases} \tilde{g}_1(d) = \tilde{g}_1(d_1) + \tilde{g}'_1(d_1)(d - d_1) + \frac{\tilde{g}''_1(d_1)(d - d_1)^2}{2} + \dots, \\ \tilde{g}_2\left(\frac{1}{d}\right) = \tilde{g}_2(d_2) + \tilde{g}'_2(d_2)\left(\frac{1}{d} - d_2\right) \\ + \frac{\tilde{g}''_2(d_2)((1/d) - d_2)^2}{2} + \dots, \end{cases} \quad (7)$$

where d_1 and d_2 are two constants. The snake normally approaches the real boundary consistently and dynamically, indicating that the evolution of the snake can be linearised. Thus, the higher order terms (≥ 2) in the Taylor series can be ignored.

Assuming the snake starts from an initial guess, then the terms with no relation to the variable d (shown in Eq. (7)) will be initially set to zero. It should be noted that during the iteration these terms may, or may not, be zero. However, setting these terms to zero will avoid the side-effects of these constant terms during the evolution (e.g. slow convergence), and hence improve the speed of convergence towards the ideal contour. Consequently, Eq. (6) has a deformable style, as defined by

$$\tilde{\alpha}dC''(s) - \frac{\tilde{\beta}}{d}C'''(s) + \gamma V = 0, \quad (8)$$

where $\tilde{\alpha} = \tilde{g}_1(d_1)$, $\tilde{\beta} = \tilde{g}_2(d_2)$, and both are constants in practice.

3.2. Mean shift constrained segmentation

As mentioned above, when matched, the snake and the real contour must share a common centroid. Alternatively, having a common centroid is a necessary condition for registration of the two contours. In this section, we investigate how to drive the centroids of the two contours towards the same settlement while performing contour segmentation. To do so, we exploit the mean shift algorithm [22]. In particular, the CAMSHIFT algorithm [23] is used due to its ability of accounting for dynamically changing distributions during the evolution. First, we briefly review the principle of mean shift.

Given an image point sequence s_i ($i = 1, 2, \dots, n$) in the m -dimensional space R^m , the multivariate kernel density estimate with kernel $K(s)$ and window radius r is given as

$$F(\mathbf{s}) = \frac{1}{nr^m} \sum_{i=1}^n K\left(\frac{\mathbf{s} - \mathbf{s}_i}{r}\right). \quad (9)$$

- | |
|---|
| <ol style="list-style-type: none"> 1. Initialisation of a contour and the corresponding parameters; 2. Make a guess for the centroid of the real contour; 3. Employment of the standard GVF scheme for evolving the contour; 4. Computation of the centroid of the evolving contour; 5. Computation of the Euclidean distance between the two centroids; 6. Apply the revised GVF strategy (Eq. (8)); 7. Conduct the standard CAMSHIFT process; 8. Evaluation: <ul style="list-style-type: none"> If the Euclidean distance between the centroids < 0.1 pixel
Stop segmentation. Otherwise
Continue with steps 3-8. |
|---|

Fig. 2. Summary of the proposed image segmentation algorithm.

The multivariate *Epanechnikov* kernel can be estimated by

$$K_E(\mathbf{s}) = \begin{cases} \frac{(m+2)(1 - \|\mathbf{s}\|^2)}{2c_m}, & \|\mathbf{s}\| < 1 \\ 0, & \text{otherwise} \end{cases} \quad (10)$$

where c_m is the volume of the unit m -dimensional sphere.

Assuming a kernel $\Psi(\mathbf{s}) = c_0 \psi(\|\mathbf{s}\|^2)$, where c_0 is a normalisation constant, the mean shift vector is expressed as

$$MS(\mathbf{s}) \equiv \frac{\sum_{i=1}^n \mathbf{s}_i \psi(\|\mathbf{s} - \mathbf{s}_i\|/r)^2}{\sum_{i=1}^n \psi(\|\mathbf{s} - \mathbf{s}_i\|/r)^2} - \mathbf{s}, \quad (11)$$

where $\psi(\cdot)$ is an intermediate function [24]. The mean shift procedure is a recursive evolution that involves the computation of the mean shift vector $MS(\mathbf{s})$ and adjustment of the centroid of kernel Ψ by $MS(\mathbf{s})$. In theory, the Euclidean distance between the centroids d is proportional to the mean of the mean shift:

$$d \propto MS(\mathbf{s})^m. \quad (12)$$

The application of the mean shift in our algorithm is straightforward. The mean shift algorithm is employed to find the contour candidate that is the most similar to the real boundary, with the similarity being expressed by the Euclidean distance between the initial centroid of the snake and that of the real boundary, which satisfies the object energy function as well. The following steps are performed: The centroid (x_c, y_c) of a contour is calculated by

$$\begin{cases} x_c = \frac{M_{10}}{M_{00}}, \\ y_c = \frac{M_{01}}{M_{00}}, \end{cases} \quad (13)$$

where we have the initial (zeroth) moment M_{00} , the moment M_{10} for x -coordinates, and the moment M_{01} for y -coordinates of image points on the contour.

The initial centroid (normally it is the centre of the image or an estimate provided by the user) for the real boundary, and the estimated one for the snake, are obtained, respectively. Once the centroids are obtained, the Euclidean distance d between these two centroids then becomes defined, which is used in Eq. (8) for performing the revised GVF strategy. This is followed by executing the standard CAMSHIFT algorithm [23,25], where Eq. (11) is deployed. After CAMSHIFT, we again compute the Euclidean distance between the centroids. Then, the extended GVF and CAMSHIFT are subsequently applied. The above procedure is iterated until the Euclidean distance of the centroids becomes smaller than 0.1. The entire algorithm is summarised in Fig. 2.

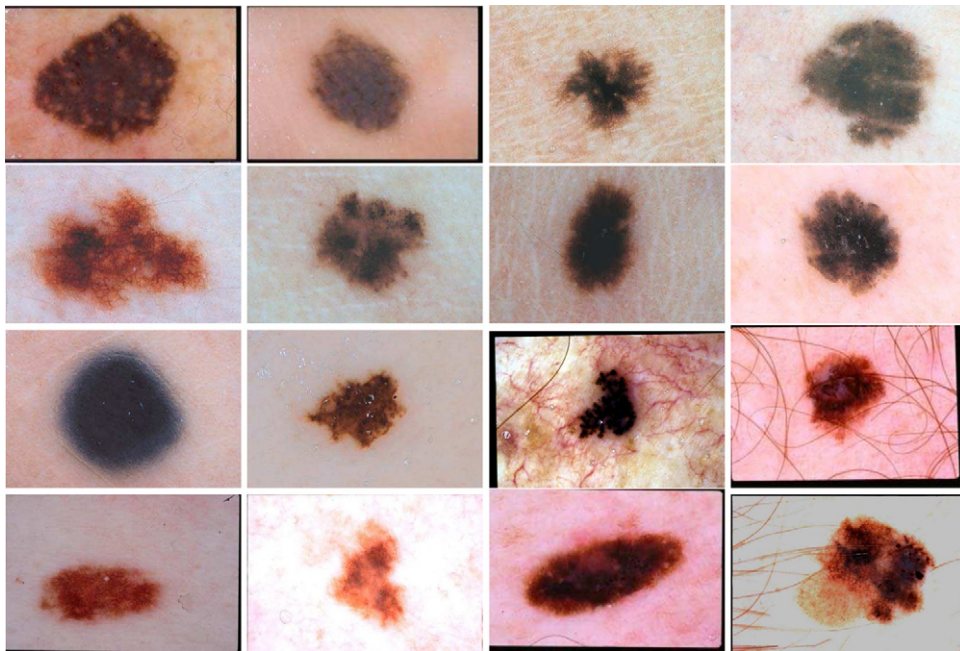


Fig. 3. Examples of test skin cancer images. These images are labeled as no. 5, 10, 15, 20, . . . , 80 (left to right along with raster direction).

3.3. Convergence properties

Let K be a function in $L_1(R^t)$ with $\int K=1$, and Eq. (9) can be regarded as

$$\tilde{q}_i \tilde{f}_i(z) = (nh_n^t)^{-1} \sum_{j=1}^n K\left(\frac{z-Z_j}{h_n}\right) I, \tag{14}$$

where n iterations will be performed in order to describe the evolving behaviour of the overall image points. $\tilde{q} \tilde{f}(z) = \max_i \tilde{q}_i \tilde{f}_i(z)$, and I is the indicator function that returns 1 for the pixels belonging to the target, and 0 for all other pixels. Eq. (14) fully determines the probability density of the registration between the contour candidate and the real contour: given a number of iterations, it finds a solution (the settlement of the contour), which is very close

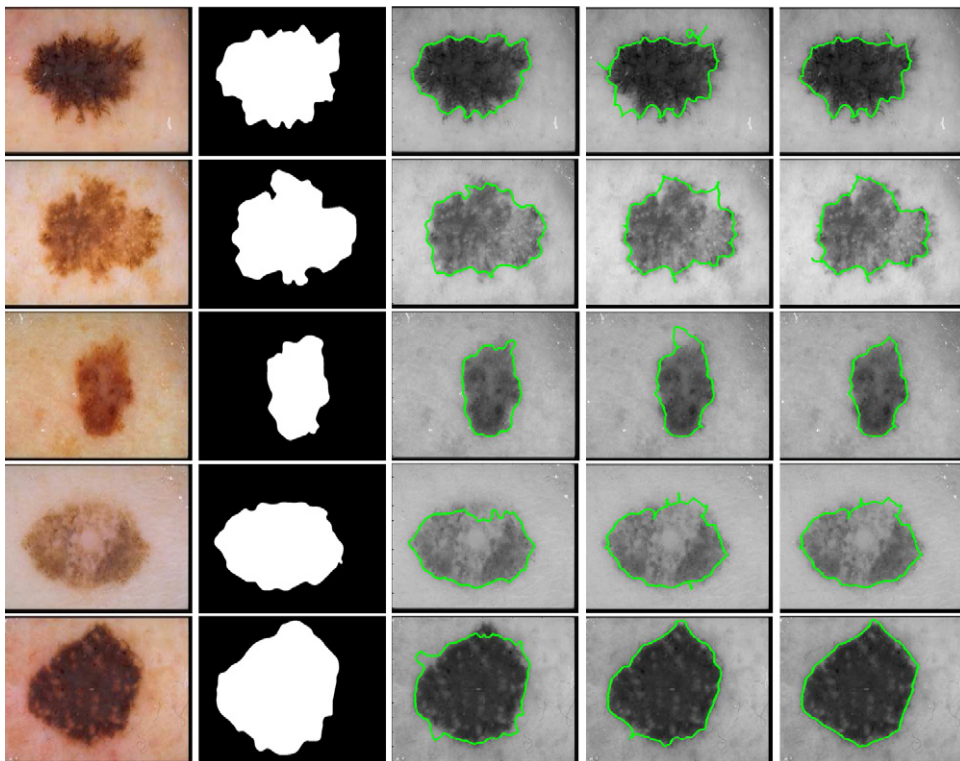


Fig. 4. Performance comparison of different segmentation algorithms in group 1: column (1) original, (2) ground truth, (3) level set, (4) classical GVF and (5) proposed.

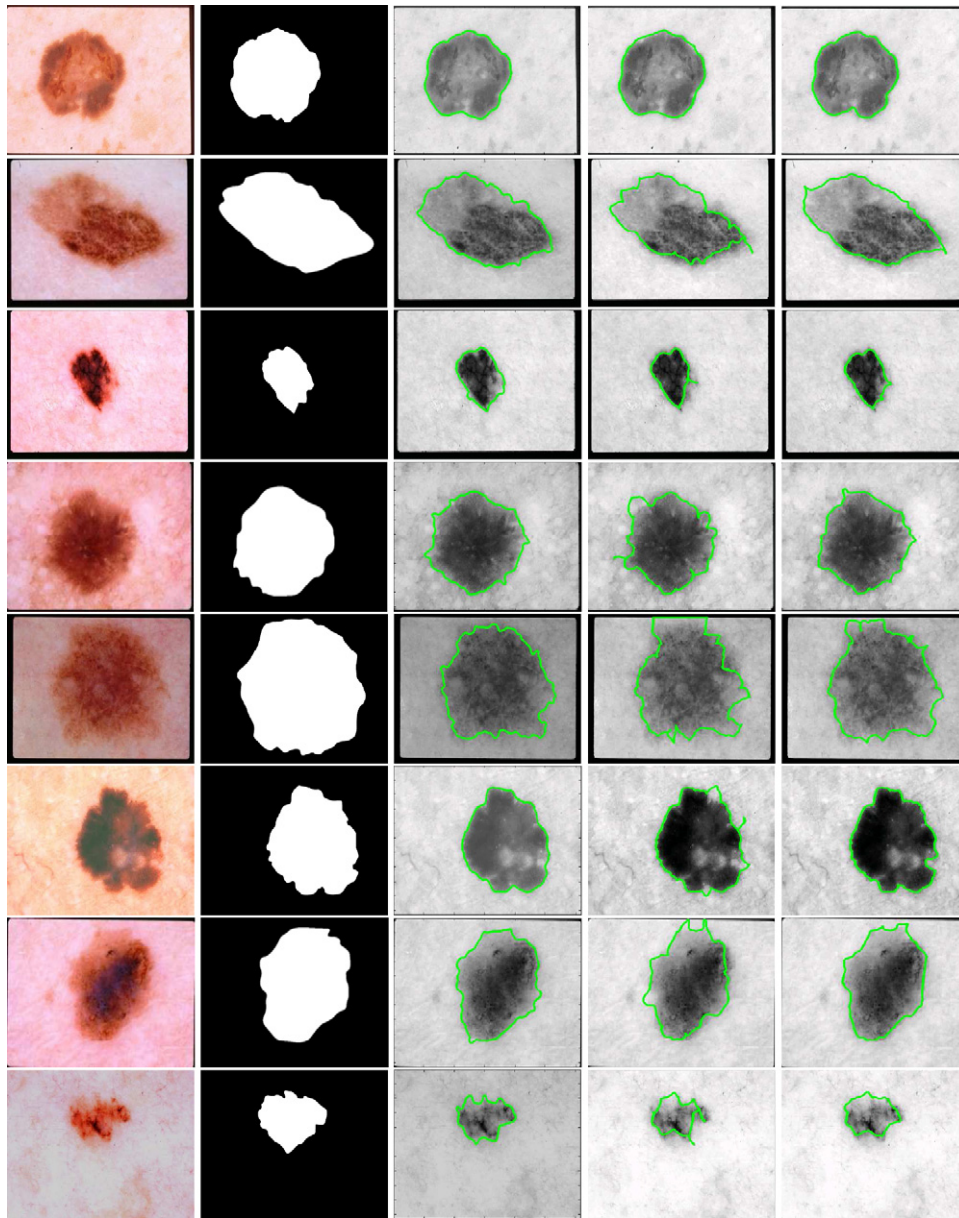


Fig. 5. Performance comparison of different segmentation algorithms in group 2: column (1) original, (2) ground truth, (3) level set, (4) classical GVF and (5) proposed.

to the real contour. This can be proved by using the following theorem:

Theorem 1. *If Z has a density, $h_v \rightarrow 0$ and $vh_v^t \rightarrow \infty$ (v is the number of iterations), then Eq. (14) satisfies: for all $\varepsilon \in (0, 1)$ there exists $v_0 > 0$ such that $P(L_v - L^* > \varepsilon) \leq \exp(-\tilde{c}v\varepsilon^2)$, where $v \geq v_0$ and \tilde{c} is a positive constant only depending on K .*

The proof for this theorem has been given in [26] (pages 257–258). In theory, this theorem explicitly reveals that there always exists an optimal solution whose probability P approaches that of the real solution.

Theorem 2. *Suppose the mean shift based GVF snake has continuous derivatives. Then, the evolution of the snake is bound in each iteration.*

To prove this theorem, one can take derivatives for both sides of Eq. (14) with respect to z . Taking into account Eq. (10), it is clear that the derivative of the right side of Eq. (14) has a definite boundary

θ , which is

$$-Z_j(2c_mnh_n^{t+1})^{-1}(m+2)I \leq \theta \leq 0. \tag{15}$$

This theorem verifies that the proposed snake will not be divergent in iteration, and the diffuse forces exist to drive the snake towards the real contour.

The above two theorems are related to the characteristics of the mean shift procedure. The following theorem is concerned with the feature of the extended GVF model (Eq. (8)).

Theorem 3. *Let the GVF snake have continuous derivatives. The evolution of the snake has efficient convergence.*

There are two coherent stages for the proof of this theorem. Firstly, we need to prove that Eq. (8) is convergent in terms of its settlement. Secondly, the convergence must be proved to be fast. The proposed GVF algorithm mainly involves the calculation of the Euclidean distance between the two consecutive centroids. Therefore, the discussion of the convergence is based on this distance.

Table 1

Segmentation performance on the complete dermoscopy image set. For each algorithm the median sensitivity and specificity are given. Values in parentheses indicate standard deviations of the measures.

Algorithm	Specificity	Sensitivity
Classical GVF	0.99 (0.10)	0.74 (0.13)
Level sets	0.99 (0.07)	0.76 (0.09)
Proposed	0.99 (0.08)	0.81 (0.09)

We can generate a derivative for the left hand side of Eq. (8) w.r.t. d , and then set the derivation to zero. This results in

$$\tilde{\alpha}C''(s) + \frac{\tilde{\beta}}{d^2}C'''(s) = 0. \quad (16)$$

Thus, the distance d is determined by

$$|d| = \sqrt{-\frac{\tilde{\beta}C'''(s)}{\tilde{\alpha}C''(s)}}. \quad (17)$$

The continuity of the derivatives have inferred that $C''(s)$ is non-zero. Therefore, the proposed GVF has a certain convergence. In the meantime, it is observed that the distance d depends on the 2nd and 4th order derivatives of the contour. Clearly, the 4th order derivative will dominate the speed of the distance value and hence the convergence is fast.

4. Experimental work

The proposed segmentation algorithm was evaluated on a set of 100 dermoscopy images (30 invasive malignant melanoma and 70 benign) obtained from the EDRA Interactive Atlas of Dermoscopy [2] and the dermatology practices of Dr. A. Marghoob (New York, NY), Dr. H. Rabinovitz (Plantation, FL) and Dr. S. Meznies (Sydney, Australia). The benign lesions included nevocellular nevi and dysplastic nevi. A subset of the images is shown in Fig. 3. Manual borders were obtained by selecting a number of points on the lesion border, connecting these with a 2nd-order B-spline and finally filling the resulting closed curve. Manual borders were determined by dermatologists Dr. W. Stoecker, Dr. J. Malters, and Dr. J. Grichnik using this method and serve as a ground truth for the experiments. The algorithms that we compared are the classical GVF [10], level set segmentation [14] and the proposed GVF algorithm.

The first group of the segmentations obtained by the various algorithms is given in Fig. 4, which shows one of the ground truth segmentations together with the results by all three methods. In general, the proposed segmentation scheme has the best performance in terms of accuracy. For example, in the first row the classical GVF algorithm leads to too much noise in the contour. The result of the level set framework is very similar to that of the proposed algorithm, where both closely outline the real boundaries of the lesions. The results shown in the third row illustrate that for this image both GVF based schemes provide similar results except for Images 2 and 3, while the level set leads to over-segmentation.

In the second test group the images are more complicated. For example, in the examples shown in rows 3 and 8 of Fig. 5 the edges of the test images do not differ significantly from their surroundings. Fig. 5 also demonstrates that the proposed algorithm is clearly better than the other two algorithms, e.g. rows 3, 4, 6 and 7. In a few cases, the classical GVF (rows 1 and 2) and level set schemes (row 5) give better results. However, in these cases, the differences between our proposed algorithm and the level set scheme are practically negligible.

Finally, in Table 1 we give the results over the complete dataset of 100 dermoscopy images in terms of median sensitivity and specificity. The figure denotes the average of the median sensitivity/specificity against the three manual borders (i.e. the average of

the three median values where each of the median values comes from 1 set of 100 manual borders). Table 1 confirms that the proposed algorithm performs better than the other two.

5. Conclusions

GVF based algorithms have been frequently used to segment medical images, but also need further development to improve segmentation accuracy. In this paper we have introduced a new mean shift based GVF segmentation algorithm for segmenting skin lesions in dermoscopy images. The proposed method incorporates a mean field term within the standard GVF objective function. Experimental results on a large dataset of 100 dermoscopy images have shown that the proposed segmentation technique is capable of providing more accurate segmentation results than classical GVF and level set schemes.

Acknowledgments

The authors would like to thank the anonymous reviewers for constructive comments that helped in improving the quality of this manuscript.

References

- [1] Jemal A, Siegel R, Ward E, Hao Y, Xu J, Thun M. Cancer statistics, 2009. *CA Cancer J Clin* 2009;59(4):225–49.
- [2] Argenziano G, Soyer H, De Giorgi V. *Dermoscopy: a tutorial*. EDRA Medical Publishing & New Media; 2002.
- [3] Steiner K, Binder M, Schemper M, Wolff K, Pehamberger H. Statistical evaluation of epiluminescence dermoscopy criteria for melanocytic pigmented lesions. *J Am Acad Dermatol* 1993;29(4):581–8.
- [4] Binder M, Schwarz M, Winkler A, Steiner A, Kaider A, Wolff K, et al. Epiluminescence microscopy. A useful tool for the diagnosis of pigmented skin lesions for formally trained dermatologists. *Arch Dermatol* 1995;131(3):286–91.
- [5] Celebi ME, Kingravi HA, Uddin B, Aslandogan YA, Stoecker WV, Moss RH. A methodological approach to the classification of dermoscopy images. *Comput Med Imaging Graph* 2007;31(6):362–73.
- [6] Celebi ME, Iyatomi H, Schaefer G, Stoecker WV. Lesion border detection in dermoscopy images. *Comput Med Imaging Graph* 2009;33(2):148–53.
- [7] Cohen L. On active contour models and balloons. *CVGIP: Image Underst* 1991;53(2):211–8.
- [8] Cohen L, Cohen I. Finite element methods for active contour models and balloons for 2D and 3D images. *IEEE Trans Pattern Anal Mach Intell* 1993;15:1131–47.
- [9] Cremers D, Tischhäuser F, Weickert J, Schnörr C. Diffusion snakes: introducing statistical shape knowledge into the Mumford-Shah functional. *Int J Comput Vis* 2002;50(3):295–313.
- [10] Xu C, Prince J. Snakes, shapes, and gradient vector flow. *IEEE Trans Image Process* 1998;7(3):359–69.
- [11] Xu C, Prince J. Generalized gradient vector flow external forces for active contours. *Signal Process* 1998;71(2):131–9.
- [12] Liu T, Zhou H, Lin F, Pang Y, Wu J. Improving image segmentation by gradient vector flow and mean shift. *Pattern Recogn Lett* 2008;29(1):90–5.
- [13] Paragios N, Mellina-Gottardo O, Ramesh V. Gradient vector flow fast geometric active contours. *IEEE Trans Pattern Anal Mach Intell* 2004;26(3):402–7.
- [14] Li C, Liu J, Fox M. Segmentation of edge preserving gradient vector flow: an approach toward automatically initializing and splitting of snakes. In: *IEEE international conference on computer vision and pattern recognition*. 2005. p. 162–7.
- [15] Chuang C-H, Lie W-N. A downstream algorithm based on extended gradient vector flow field for object segmentation. *IEEE Trans Image Process* 2004;13(10):1379–92.
- [16] Yang C, Duraiswami R, Davis L. Efficient mean-shift tracking via a new similarity measure. In: *IEEE international conference on computer vision and pattern recognition (CVPR)*. 2005. p. 176–83.
- [17] Vasilevskiy A, Siddiqi K. Flux maximizing geometric flows. *IEEE Trans Pattern Anal Mach Intell* 2002;24(12):1565–78.
- [18] Caselles V, Kimmel R, Sapiro G. Geodesic active contour. In: *IEEE int'l conf. comput. vis*. 1995. p. 694–9.
- [19] Kass M, Witkin A, Terzopoulos D. Snakes: active contour models. In: *Proceedings of the international conference on computer vision*. 1987. p. 259–68.
- [20] Zhou H, Liu T, Hu H, Pang Y, Lin F, Wu J. A hybrid framework for image segmentation. In: *Proceedings of the IEEE international conference on acoustics, speech, and signal processing*. 2005. p. 749–52.
- [21] Zhou H, Liu T, Lin F, Pang Y, Wu J. Segmentation of complex shapes by adaptive energy forces. In: *Proceedings of the 13th international conference in Central*

- Europe on computer graphics, visualization and computer vision (poster). 2005. p. 79–80.
- [22] Cheng Y. Mean shift, mode seeking, and clustering. *IEEE Trans Pattern Anal Mach Intell* 1995;17:790–9.
- [23] Bradski G. Computer vision face tracking for use in a perceptual user interface. In: *IEEE workshop on applications of computer vision*. 1998. p. 214–9.
- [24] Comaniciu D, Ramesh V, Meer P. Real-time tracking of non-rigid objects using mean shift. In: *Proceedings of the computer vision and pattern recognition*. 2000. p. 142–9.
- [25] Wang J, Thiesson B, Xu Y, Cohen M. Image and video segmentation by anisotropic kernel mean shift. In: *Proceedings of the European conference on computer vision*. 2004. p. 238–49.
- [26] Devroye L, Györfi L. *Nonparameteric density estimation*. John Wiley & Sons; 1985.